INTERNATIONAL JOURNAL FOR NUMERICAL METHODS IN FLUIDS
Int. J. Numer. Meth. Fluids 2007; **55**:565–587
Published online 20 March 2007 in Wiley InterScience (www.interscience.wiley.com). DOI: 10.1002/fld.1477

A continuous second-order sensitivity equation method for time-dependent incompressible laminar flows

F. Ilinca[1,*,†], D. Pelletier[2] and J. Borggaard[3]

[1]*National Research Council, 75 de Mortagne, Boucherville, Que., Canada J4B 6Y4*
[2]*École Polytechnique de Montréal, Montréal, Que., Canada H3C 3A7*
[3]*Virginia Tech, Blacksburg, VA 24061-0531, U.S.A.*

SUMMARY

This paper presents a general formulation of the continuous sensitivity equation method (SEM) for computing first- and second-order sensitivities of time-dependent, incompressible laminar flows. The formulation accounts for complex parameter dependence and is suitable for a wide range of problems. The SEM formulation is verified on a problem with a closed-form solution. Systematic grid convergence studies confirm the theoretical rates of convergence in both space and time. The methodology is then applied to uniform flow around a circular cylinder. The flow starts with a symmetrical solution and transitions to the traditional Von Karman street (alternate vortex shedding). Sensitivities are used to demonstrate fast evaluation of nearby flows. The accuracy of nearby flows is much improved when second-order sensitivities are used. The sensitivity of the Strouhal number with respect to the Reynolds number agrees well with the computed and experimental *St–Re* relationship. Copyright © 2007 John Wiley & Sons, Ltd.

Received 1 November 2006; Revised 8 February 2007; Accepted 8 February 2007

KEY WORDS: sensitivity equations; second-order sensitivity; 3D finite elements; time-dependent flows; incompressible flows

1. INTRODUCTION

An engineer using CFD for design must answer two questions: are the flow predictions obtained with CFD accurate enough for design purposes? and what are the consequences of changing the parameters controlling the system (boundary conditions, shape parameters, etc.)? This paper

*Correspondence to: F. Ilinca, National Research Council, Industrial Materials Institute, 75 de Mortagne, Boucherville, Que., Canada J4B 6Y4.
†E-mail: florin.ilinca@cnrc-nrc.gc.ca

Contract/grant sponsor: NSERC
Contract/grant sponsor: Canada Research Chair Program
Contract/grant sponsor: Air Force Office of Scientific Research (AFOSR); contract/grant number: F49620-00-1-0299

presents a general continuous sensitivity equation method (SEM) for time-dependent incompressible laminar flows as a means of answering the latter question. The former issue is best dealt with by a comprehensive verification studies including systematic time-step and grid refinement [1] and validation by a comparison to experimental measurements.

A sensitivity is the derivative of a dependent variable with respect to a model parameter. For the flow around an airfoil, $\partial u/\partial \alpha$ is the sensitivity of the velocity with respect to the airfoil angle of attack. It expresses how the velocity field responds to perturbations of α around its nominal value. Sensitivity information can also be used for fast evaluation of nearby flows without resorting to a full blown flow re-analysis. This is done *via* the Taylor series expansions in parameter space, and is especially useful to answer *what if questions* for complex flows. Finally, sensitivity information can serve to cascade input data uncertainty through a CFD code to yield uncertainty estimates of the flow response. In both cases, cost-effectiveness is achieved because sensitivities are obtained at a fraction of the cost of computing the flow.

There are several means of computing flow sensitivities: finite differences of flow solutions, the complex step method [2], automatic differentiation [3], and SEMs [4–6]. The first option is costly because the problem must be solved for two or more values of each parameter of interest. Furthermore, technical problems arise because non-matching meshes are obtained for different values of a shape parameter. The complex-step method is code invasive: it requires a complete rewrite of the software in complex variables. While this can be automated, it has a significant impact on performance. Automatic differentiation is equivalent to differentiating the discrete equations to generate a system of equations for the discrete sensitivities. It is powerful because it automatically generates the code for calculating sensitivities. In many cases, implementation requires human intervention to ensure efficiency of the resulting sensitivity code. Approaches to calculating sensitivities also differ depending on the order of the operations of approximation and differentiation. In the *discrete* sensitivity equation approach, the total derivative of the flow approximation with respect to the parameter is calculated [7], whereas in the *continuous* SEM one differentiates the continuum equations to yield differential equations for the continuous sensitivities [4]. See Hien and Kleiber [8] for a discussion of the two approaches. We have adopted the latter approach.

Sensitivity analysis is a more advanced field in solid mechanics than in fluid dynamics. Indeed, textbooks have been written on sensitivity analysis of structures [7, 8]. To our knowledge, there is only one book on sensitivity analysis of flow problems [5]. It is rather recent and more specialized than structural mechanics books. Gunzburger [9] discusses sensitivity analysis in the context of flow control and optimization.

Automatic differentiation for first-order flow sensitivities is discussed by Sherman *et al.* [10] and Putko *et al.* [3]. Continuous SEMs may be found in Godfrey *et al.* [11, 12], Borggaard and Burns [4], Limache [13] and Turgeon [14] for aerodynamics problems. Application to heat conduction is reported by Blackwell *et al.* [15]. Sensitivities for incompressible flows with heat transfer may be found in several references [6, 16–18]. Sensitivity analysis for turbulence models is detailed in the works by Godfrey and Cliff [12] and Turgeon *et al.* [19, 20]. Solution of the sensitivity equations for the transient incompressible flow of non-Newtonian fluids is presented by Ilinca and Hétu [21]. A wide variety of flow regimes were treated by the authors [6, 17, 18, 20, 22, 23]. This body of work has shown that sensitivities provide an enriched base of information on which to develop an understanding of complex flow problems. The work presented here is an extension to second-order sensitivities of the methodology developed previously for time-dependent flows [24].

The paper is organized as follows. First, we present the equations describing time-dependent laminar flow along with their boundary and initial conditions. The first- and second-order sensitivity

DOI: 10.1002/fld

equations and their boundary/initial conditions are then described in detail. The methodology and its finite element solver are verified on a problem possessing a closed form solution. The approach is then applied to the flow around a circular cylinder. Several uses of sensitivities are demonstrated. Emphasis is put on the *St–Re* relationship and the computed sensitivity of the Strouhal number. The paper ends with conclusions.

2. FLOW EQUATIONS

2.1. Navier–Stokes equations

The flow regime of interest is modelled by the momentum and continuity equations:

$$\rho\frac{\partial \mathbf{u}}{\partial t} + \rho\mathbf{u}\cdot\nabla\mathbf{u} = -\nabla p + \mathbf{f} + \nabla\cdot[2\mu\boldsymbol{\gamma}(\mathbf{u})] \tag{1}$$

$$\nabla\cdot\mathbf{u} = 0 \tag{2}$$

where ρ is the density, $\mathbf{u}$ is the velocity, p is the pressure, μ is the viscosity, t represents time, $\boldsymbol{\gamma}(\mathbf{u}) = (\nabla\mathbf{u} + \nabla\mathbf{u}^{\mathrm{T}})/2$ is the shear rate tensor and $\mathbf{f}$ is a body force. The above system is closed with a proper set of initial conditions

$$\mathbf{u}(\mathbf{x}, t=0) = \mathbf{U}_0(\mathbf{x}) \quad \text{in } \Omega \tag{3}$$

and the Dirichlet and Neumann boundary conditions

$$\mathbf{u}(\mathbf{x}, t) = \mathbf{U}_D(\mathbf{x}, t) \quad \text{on } \Gamma_D \tag{4}$$

$$\mathbf{t} = [-p\mathbb{I} + 2\mu\boldsymbol{\gamma}(\mathbf{u})]\cdot\hat{\mathbf{n}} = \mathbf{F}^N \quad \text{on } \Gamma_N \tag{5}$$

where $\mathbf{U}_D$ is the value of the velocity imposed along the boundary Γ_D, $\mathbb{I}$ is the identity tensor and $\mathbf{F}^N$ is the imposed boundary value of the surface traction force $\mathbf{t}$.

3. SENSITIVITY EQUATIONS

3.1. General formulation of first-order sensitivity equations

The continuous sensitivity equations (CSEs) are derived formally by implicit differentiation of the flow equations (1) and (2) with respect to parameter a. We treat the flow variable $\mathbf{u}$ and p as functions of space, time and of the parameter a. This dependence is denoted as $\mathbf{u}(\mathbf{x}, t; a)$ and $p(\mathbf{x}, t; a)$. The velocity and pressure sensitivities are defined as the partial derivatives $\mathbf{s}_u^a = \partial\mathbf{u}/\partial a$ and $s_p^a = \partial p/\partial a$, whereas the derivatives of the fluid properties and other flow parameters are denoted by a $(')$ and the subscript a (as example $\mu_a' = \partial\mu/\partial a$ for the sensitivity of the viscosity). Differentiation of Equations (1) and (2) yields

$$\rho_a'\left(\frac{\partial\mathbf{u}}{\partial t} + \mathbf{u}\cdot\nabla\mathbf{u}\right) + \rho\left(\frac{\partial\mathbf{s}_u^a}{\partial t} + \mathbf{u}\cdot\nabla\mathbf{s}_u^a + \mathbf{s}_u^a\cdot\nabla\mathbf{u}\right)$$
$$= -\nabla s_p^a + \mathbf{f}_a' + \nabla\cdot[2\mu_a'\boldsymbol{\gamma}(\mathbf{u}) + 2\mu\boldsymbol{\gamma}(\mathbf{s}_u^a)] \tag{6}$$

$$\nabla\cdot\mathbf{s}_u^a = 0 \tag{7}$$

DOI: 10.1002/fld

3.2. General formulation of second-order sensitivity equations

The same approach is applied to obtain second-order sensitivity equations. Here, we consider two independent parameters a and b. Thus, $\mathbf{u}$ can be written as $\mathbf{u}(\mathbf{x}, t; a, b)$. Second-order flow sensitivities are defined as the partial derivatives $\mathbf{s}_u^{ab} = \partial^2\mathbf{u}/\partial a\partial b$ and $s_p^{ab} = \partial^2 p/\partial a\partial b$, and denoting the second-order derivatives of the fluid properties and other flow parameters by a ($''$) and the subscript ab, differentiation of Equations (1) and (2) yields

$$\begin{aligned}
&\rho''_{ab}\left(\frac{\partial\mathbf{u}}{\partial t} + \mathbf{u}\cdot\nabla\mathbf{u}\right) + \rho'_a\left(\frac{\partial\mathbf{s}_u^b}{\partial t} + \mathbf{u}\cdot\nabla\mathbf{s}_u^b + \mathbf{s}_u^b\cdot\nabla\mathbf{u}\right)\\
&\quad + \rho'_b\left(\frac{\partial\mathbf{s}_u^a}{\partial t} + \mathbf{u}\cdot\nabla\mathbf{s}_u^a + \mathbf{s}_u^a\cdot\nabla\mathbf{u}\right)\\
&\quad + \rho\left(\frac{\partial\mathbf{s}_u^{ab}}{\partial t} + \mathbf{u}\cdot\nabla\mathbf{s}_u^{ab} + \mathbf{s}_u^b\cdot\nabla\mathbf{s}_u^a + \mathbf{s}_u^a\cdot\nabla\mathbf{s}_u^b + \mathbf{s}_u^{ab}\cdot\nabla\mathbf{u}\right)\\
&\qquad = -\nabla s_p^{ab} + \mathbf{f}''_{ab}\\
&\qquad\quad + \nabla\cdot[2\mu''_{ab}\boldsymbol{\gamma}(\mathbf{u}) + 2\mu'_b\boldsymbol{\gamma}(\mathbf{s}_u^a) + 2\mu'_a\boldsymbol{\gamma}(\mathbf{s}_u^b) + 2\mu\boldsymbol{\gamma}(\mathbf{s}_u^{ab})] \qquad (8)
\end{aligned}$$

$$\nabla\cdot\mathbf{s}_u^{ab} = 0 \qquad (9)$$

Similar equations are derived for the second-order sensitivities $\mathbf{s}_u^{aa} = \partial^2\mathbf{u}/\partial a^2$ and $\mathbf{s}_u^{bb} = \partial^2\mathbf{u}/\partial b^2$.

3.3. Initial and boundary conditions

Initial conditions for the sensitivity equations are obtained by implicit differentiation of Equation (3)

$$\mathbf{s}_\mathbf{u}^a(\mathbf{x}, t=0) = \frac{\partial\mathbf{U}_0}{\partial a}(\mathbf{x}) \quad \text{in } \Omega \qquad (10)$$

$$\mathbf{s}_\mathbf{u}^{ab}(\mathbf{x}, t=0) = \frac{\partial^2\mathbf{U}_0}{\partial a\partial b}(\mathbf{x}) \quad \text{in } \Omega \qquad (11)$$

Boundary conditions are obtained in a similar manner and can be written as

$$s_\mathbf{u}^a = \frac{\partial\mathbf{U}_D}{\partial a} \quad \text{on } \Gamma_D \qquad (12)$$

$$\frac{\partial\mathbf{t}}{\partial a} = [-s_p^a\mathbb{I} + 2(\mu\boldsymbol{\gamma}(s_\mathbf{u}^a) + \mu'_a\boldsymbol{\gamma}(\mathbf{u}))]\cdot\hat{\mathbf{n}} = \frac{\partial\mathbf{F}^N}{\partial a} \quad \text{on } \Gamma_N \qquad (13)$$

for the first-order sensitivities. Similar expressions are derived for the sensitivity with respect to the parameter b. Further differentiation of Equations (12) and (13) provides the boundary conditions for the second-order sensitivities $s_\mathbf{u}^{aa}$, $s_\mathbf{u}^{ab}$, and $s_\mathbf{u}^{bb}$. For example, we obtain

$$s_\mathbf{u}^{ab} = \frac{\partial^2\mathbf{U}_D}{\partial a\partial b} \quad \text{on } \Gamma_D \qquad (14)$$

$$\frac{\partial^2\mathbf{t}}{\partial a\partial b} = [-s_p^{ab}\mathbb{I} + 2(\mu\boldsymbol{\gamma}(s_\mathbf{u}^{ab}) + \mu'_a\boldsymbol{\gamma}(s_\mathbf{u}^b) + \mu'_b\boldsymbol{\gamma}(s_\mathbf{u}^a) + \mu''_{ab}\boldsymbol{\gamma}(\mathbf{u}))]\cdot\hat{\mathbf{n}} = \frac{\partial^2\mathbf{F}^N}{\partial a\partial b} \quad \text{on } \Gamma_N \qquad (15)$$

DOI: 10.1002/fld

4. IMPLEMENTATION

There are many choices possible for solving the flow and sensitivity equations. In theory one can solve the CSE by any numerical method. In practice, it is convenient and cost effective to use the same finite element method for the flow and the CSE. Indeed, note that the CSE amount to a Newton linearization of the Navier–Stokes equations. Thus, if one uses Newton's method for solving the finite element equations for the flow, the flow sensitivity equations will have the same finite element matrix. Only the right-hand side will differ. This results in substantial savings since the matrix of the first- and second-order sensitivities need not be recomputed. In practice, the solution for the sensitivity with respect to one parameter is obtained at approximately 10% of the cost of solving the flow equations.

In the cases considered previously by Mahieu *et al.* [25], quadratic elements were used to solve flows at Reynolds numbers low enough to justify using the Galerkin finite element method for both the flow and sensitivity equations. No stabilization was required. However, our long-term goal is sensitivity analysis of a large spectrum of 3D flow problems. For simplicity, robustness and cost-effectiveness of the simulations we use equal-order interpolation for velocity and pressure (P1–P1 tetrahedral elements) that need stabilization terms to avoid velocity–pressure decoupling [26–28]. Stabilization can also avoid spurious oscillations in the case of convection-dominated flows. In this work, the flow equations and the CSE are solved on 3D meshes by a streamline-upwind Petrov Galerkin (SUPG) finite element method [29]. Time is discretized by an implicit Euler scheme.

The SUPG variational formulation of the momentum-continuity equations is [28–30]

$$\int_\Omega \left\{ \rho\left(\frac{\partial \mathbf{u}}{\partial t} + \mathbf{u}\cdot\nabla\mathbf{u}\right) - \mathbf{f} \right\} \mathbf{v}\,\mathrm{d}\Omega - \int_\Omega p\nabla\cdot\mathbf{v}\,\mathrm{d}\Omega + \int_\Omega 2\mu\boldsymbol{\gamma}(\mathbf{u}) : \boldsymbol{\gamma}(\mathbf{v})\,\mathrm{d}\Omega$$
$$+ \sum_K \int_{\Omega_K} \left\{ \rho\left(\frac{\partial \mathbf{u}}{\partial t} + \mathbf{u}\cdot\nabla\mathbf{u}\right) + \nabla p - \nabla\cdot[2\mu\boldsymbol{\gamma}(\mathbf{u})] - \mathbf{f} \right\} \tau_u(\rho\mathbf{u}\cdot\nabla\mathbf{v})\,\mathrm{d}\Omega_K$$
$$+ \sum_K \int_{\Omega_K} \nabla\cdot\mathbf{u}\delta\nabla\cdot\mathbf{v}\,\mathrm{d}\Omega_K = \int_{\Gamma_N} \mathbf{F}^N\mathbf{v}\,\mathrm{d}\Gamma_N \tag{16}$$

$$\int_\Omega \nabla\cdot\mathbf{u}q\,\mathrm{d}\Omega + \sum_K \int_{\Omega_K} \left\{ \rho\left(\frac{\partial \mathbf{u}}{\partial t} + \mathbf{u}\cdot\nabla\mathbf{u}\right) + \nabla p - \nabla\cdot[2\mu\boldsymbol{\gamma}(\mathbf{u})] - \mathbf{f} \right\} \tau_u\nabla q\,\mathrm{d}\Omega_K = 0 \tag{17}$$

where $\mathbf{v}$ and q denote the velocity and pressure test functions, respectively, and Ω_K denotes the volume of element K. The integrals over the entire domain identify the Galerkin contribution, while the stabilization terms are integrated only on the element interiors (i.e. terms in the summations). The stabilization parameters τ_u and δ are defined as [29, 31]

$$\tau_u = \left[\left(\frac{2\rho}{\Delta t}\right)^2 + \left(\frac{2\rho|\mathbf{u}|}{h_K}\right)^2 + \left(\frac{4\mu}{m_k h_K^2}\right)^2 \right]^{-1/2} \tag{18}$$

$$\delta = \frac{h_K^2}{2\tau_u} \tag{19}$$

Here Δt is the time step, h_K is the size of the element K and m_k is a coefficient set to $1/3$ for linear elements (see References [28, 30]). A similar finite element method is applied to the solution

DOI: 10.1002/fld

of the sensitivity equations. For simplicity, we present here the sensitivities equations in the case of constant properties flows:

- *First-order sensitivities*:

$$\int_\Omega \left\{ \rho \left(\frac{\partial \mathbf{s}_u^a}{\partial t} + \mathbf{u} \cdot \nabla \mathbf{s}_u^a + \mathbf{s}_u^a \cdot \nabla \mathbf{u} \right) - \mathbf{f}'_a \right\} \mathbf{v} \, \mathrm{d}\Omega - \int_\Omega s_p^a \nabla \cdot \mathbf{v} \, \mathrm{d}\Omega + \int_\Omega 2\mu \boldsymbol{\gamma}(\mathbf{s}_u^a) : \boldsymbol{\gamma}(\mathbf{v}) \, \mathrm{d}\Omega$$
$$+ \sum_K \int_{\Omega_K} \left\{ \rho \left(\frac{\partial \mathbf{s}_u^a}{\partial t} + \mathbf{u} \cdot \nabla \mathbf{s}_u^a + \mathbf{s}_u^a \cdot \nabla \mathbf{u} \right) + \nabla s_p^a - \nabla \cdot [2\mu \boldsymbol{\gamma}(\mathbf{s}_u^a)] - \mathbf{f}'_a \right\} \tau_u (\rho \mathbf{u} \cdot \nabla \mathbf{v}) \, \mathrm{d}\Omega_K$$
$$+ \sum_K \int_{\Omega_K} \nabla \cdot \mathbf{s}_u^a \delta \nabla \cdot \mathbf{v} \, \mathrm{d}\Omega_K = \int_{\Gamma_N} \frac{\partial \mathbf{F}^N}{\partial a} \mathbf{v} \, \mathrm{d}\Gamma_N \tag{20}$$

$$\int_\Omega \nabla \cdot \mathbf{s}_u^a q \, \mathrm{d}\Omega + \sum_K \int_{\Omega_K} \left\{ \rho \left(\frac{\partial \mathbf{s}_u^a}{\partial t} + \mathbf{u} \cdot \nabla \mathbf{s}_u^a + \mathbf{s}_u^a \cdot \nabla \mathbf{u} \right) \right.$$
$$\left. + \nabla s_p^a - \nabla \cdot [2\mu \boldsymbol{\gamma}(\mathbf{s}_u^a)] - \mathbf{f}'_a \right\} \tau_u \nabla q \, \mathrm{d}\Omega_K = 0 \tag{21}$$

- *Second-order sensitivities*:

$$\int_\Omega \left\{ \rho \left(\frac{\partial \mathbf{s}_u^{ab}}{\partial t} + \mathbf{u} \cdot \nabla \mathbf{s}_u^{ab} + \mathbf{s}_u^b \cdot \nabla \mathbf{s}_u^a + \mathbf{s}_u^a \cdot \nabla \mathbf{s}_u^b + \mathbf{s}_u^{ab} \cdot \nabla \mathbf{u} \right) - \mathbf{f}'_{ab} \right\} \mathbf{v} \, \mathrm{d}\Omega$$
$$- \int_\Omega s_p^{ab} \nabla \cdot \mathbf{v} \, \mathrm{d}\Omega + \int_\Omega 2\mu \boldsymbol{\gamma}(\mathbf{s}_u^{ab}) : \boldsymbol{\gamma}(\mathbf{v}) \, \mathrm{d}\Omega$$
$$+ \sum_K \int_{\Omega_K} \left\{ \rho \left(\frac{\partial \mathbf{s}_u^{ab}}{\partial t} + \mathbf{u} \cdot \nabla \mathbf{s}_u^{ab} + \mathbf{s}_u^b \cdot \nabla \mathbf{s}_u^a + \mathbf{s}_u^a \cdot \nabla \mathbf{s}_u^b + \mathbf{s}_u^{ab} \cdot \nabla \mathbf{u} \right) \right.$$
$$\left. + \nabla s_p^{ab} - \nabla \cdot [2\mu \boldsymbol{\gamma}(\mathbf{s}_u^{ab})] - \mathbf{f}'_{ab} \right\} \tau_u (\rho \mathbf{u} \cdot \nabla \mathbf{v}) \, \mathrm{d}\Omega_K$$
$$+ \sum_K \int_{\Omega_K} \nabla \cdot \mathbf{s}_u^{ab} \delta \nabla \cdot \mathbf{v} \, \mathrm{d}\Omega_K$$
$$= \int_{\Gamma_N} \frac{\partial^2 \mathbf{F}^N}{\partial a \partial b} \mathbf{v} \, \mathrm{d}\Gamma_N \tag{22}$$

$$\int_\Omega \nabla \cdot \mathbf{s}_u^{ab} q \, \mathrm{d}\Omega + \sum_K \int_{\Omega_K} \left\{ \rho \left(\frac{\partial \mathbf{s}_u^{ab}}{\partial t} + \mathbf{u} \cdot \nabla \mathbf{s}_u^{ab} + \mathbf{s}_u^b \cdot \nabla \mathbf{s}_u^a + \mathbf{s}_u^a \cdot \nabla \mathbf{s}_u^b + \mathbf{s}_u^{ab} \cdot \nabla \mathbf{u} \right) \right.$$
$$\left. + \nabla s_p^{ab} - \nabla \cdot [2\mu \boldsymbol{\gamma}(\mathbf{s}_u^{ab})] - \mathbf{f}'_{ab} \right\} \tau_u \nabla q \, \mathrm{d}\Omega_K = 0 \tag{23}$$

DOI: 10.1002/fld

The integrals over the entire domain represent the Galerkin contribution, whereas the integrals over the element interiors represent the SUPG stabilization terms for the sensitivity equations. The solution algorithm works therefore as follows:

At each time step

- iterates over the non-linear Navier–Stokes equations (16) and (17) until convergence. A few steps of successive substitution (Picard's method) are performed at the beginning of the first time step and Newton's linearization is used afterward;
- use Newton's linearization matrix of the last iteration on the flow problem and solve the linear system for the first-order sensitivities equations (20) and (21). This step requires the evaluation of one right-hand side and a linear equation solve for each parameter;
- use the same approach for the second-order sensitivities. Again, this requires one right-hand side evaluation and one matrix solve per second-order sensitivity.

Element matrices are constructed using a numerical Jacobian technique and assembled in a compressed sparse row format. Flow and sensitivity global systems are solved by BiCG stabilized iterative methods.

5. NUMERICAL RESULTS

In this section, the numerical approach is first verified using the method of manufactured solutions (MMS) [1]. It is then applied to the uniform flow around a circular cylinder. In the verification case, a direct differentiation of the manufactured solution provides closed-form expressions for the sensitivities. A grid and time step refinement study is performed to assess the grid convergence and accuracy of the flow and sensitivity solutions.

5.1. Verification

We use the following expressions for the velocity components taken from the Stommel ocean flow model [32]

$$u(x, y) = \frac{\mathscr{F}}{R} \cos\left(\frac{\pi y}{b}\right) [C_1 \mathrm{e}^{k_1 x} + C_2 \mathrm{e}^{k_2 x} - 1] \tag{24}$$

$$v(x, y) = -\frac{b}{\pi} \frac{\mathscr{F}}{R} \sin\left(\frac{\pi y}{b}\right) [C_1 k_1 \mathrm{e}^{k_1 x} + C_2 k_2 \mathrm{e}^{k_2 x}] \tag{25}$$

with

$$k_{1,2} = -\frac{D\beta}{2R} \pm \sqrt{\left(\frac{D\beta}{2R}\right)^2 + \left(\frac{\pi}{b}\right)^2} \tag{26}$$

and

$$C_1 = \frac{1 - \mathrm{e}^{k_2 \lambda}}{\mathrm{e}^{k_1 \lambda} - \mathrm{e}^{k_2 \lambda}}, \quad C_2 = \frac{\mathrm{e}^{k_1 \lambda} - 1}{\mathrm{e}^{k_1 \lambda} - \mathrm{e}^{k_2 \lambda}} \tag{27}$$

The same problem was used by Hristova *et al.* [24] to verify the 2D solution of the flow and first-order sensitivity equations. The original Stommel solution is for a steady-state flow. By taking

$$\mathscr{F} = F \sin(\pi t) \tag{28}$$

DOI: 10.1002/fld

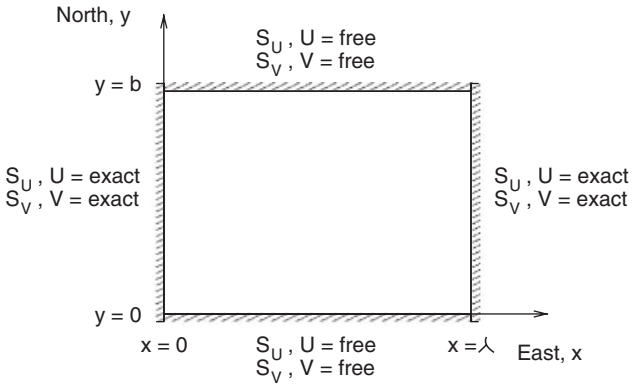

Figure 1. Verification problem: computational domain.

Table I. Parameters of the 'ocean-like' manufactured solution.

Parameter	Dimensional	Non-dimensional
Latitude (b)	$2\pi \times 10^6$ m	1.00
Longitude (λ)	10^7 m	1.59
Depth (D)	200 m	3.1831×10^{-5}
Wind force (F)	0.3×10^{-5} m^2 s^{-2}	1.9249×10^{-11}
Friction coefficient (R)	0.6×10^{-3} ms^{-1}	1.5198×10^{-6}
Coriolis effect (β)	10^{-11} m^{-1}s^{-1}	1.00

we generate a time-dependent velocity field suitable for verification of the unsteady solvers. Finally, we choose the pressure to be

$$p(x, y) = 2\mu \frac{\partial v}{\partial y} = -2 \frac{\mathscr{F}}{R} \cos\left(\frac{\pi y}{b}\right) [C_1 k_1 e^{k_1 x} + C_2 k_2 e^{k_2 x}] \tag{29}$$

so that a zero normal traction ($F_y^N = 0$ in Equation (5)) may be imposed on the top and bottom boundaries of the computational domain as shown in Figure 1. These expressions are substituted in the Navier–Stokes equations to define the body force $\mathbf{f}$ ensuring that the momentum equations (1) are satisfied [24].

The meaning and values of the various parameters are given in Table I. For simplicity, the length scale is taken as $L^* = b = 2\pi \times 10^6$ m while the timescale is $T^* = 1/\beta L^*$.

The computational domain and boundary conditions are shown in Figure 1. A grid and time step convergence study is carried out for the flow and for its first- and second-order sensitivities with respect to the following two parameters: the Coriolis coefficient β and the friction coefficient R. Analytical expressions for the sensitivities are obtained by direct differentiation of Equations (24)–(29). The required source terms $\mathbf{f}'$ and $\mathbf{f}''$ in the sensitivity equations are obtained by the differentiation of $\mathbf{f}$ in Equation (1). The grid refinement study reported here is performed for $\beta = 0$. Similar results were obtained with $\beta \neq 0$. The mesh and time steps for the grid sequence

DOI: 10.1002/fld

Table II. Mesh size and time steps for verification problem.

Mesh	h	Δt
1	0.2	0.1
2	0.1	0.05
3	0.05	0.025
4	0.025	0.0125
5	0.0125	0.00625

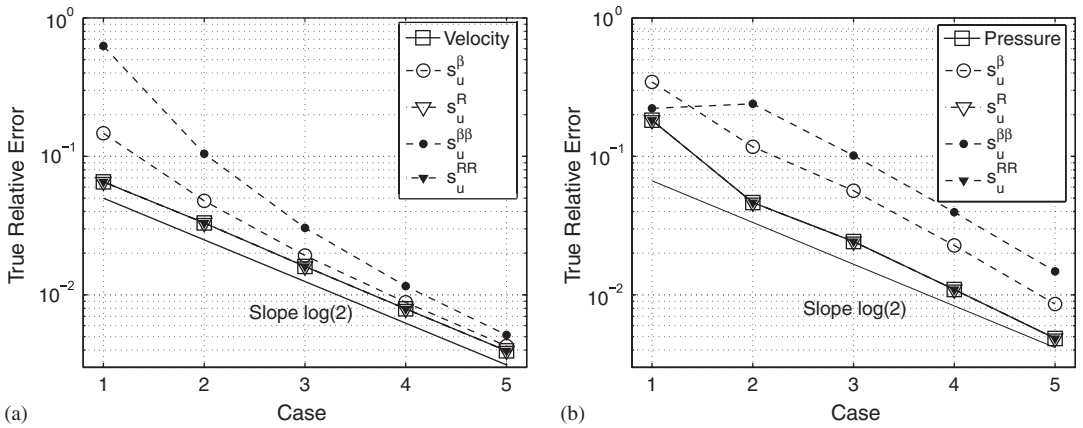

Figure 2. Verification problem; convergence of u, p and their sensitivities: (a) u and its sensitivities and (b) p and its sensitivities.

are reported in Table II. The space–time interpolation scheme is accurate to $\mathcal{O}(\delta t, \delta x)$, so if we choose to refine the time step by 2 and the mesh size by 2, the error is expected to decrease by a factor of 2 from one mesh to the next. Figure 2(a) and (b) shows the results for the velocity, the pressure and their sensitivities with respect to β and R. The continuous unmarked line has the slope of 2 and serves as a reference to asses the convergence rate. The error for the flow and its sensitivities decreases with each mesh refinement, except for the second-order sensitivity of the pressure with respect to β between meshes 1 and 2. The initial mesh (mesh 1 in Table II) is very coarse and the solution for the sensitivity is unable to capture the sharp changes in the solution at the left and right boundaries. After the first refinement, the solution recovers those boundary layers but it overestimates the solution gradient. The net result is that the error of the second-order pressure sensitivity increases with refinement. Further refinement leads to improvements in the solution of the second-order sensitivity and the error decreases from one mesh to the next. In the present case ($\beta = 0$), the exact solution for the sensitivities with respect to R is obtained by multiplying the flow solution by $-1/R$ for the first-order sensitivities and by $1/R^2$ for the second-order sensitivities. The curves for the relative error would therefore be superimposed as shown in Figure 2(a) and (b). The results indicate that optimum grid convergence is obtained for the solution sensitivities. The convergence rate for the pressure and its sensitivities is slightly

DOI: 10.1002/fld

greater than 2 on the finner meshes. This may be caused by the pressure stabilization of the P1–P1 element. Note that stabilization terms contain parameters that depend on the element mesh size and that the required amount of stabilization decreases with mesh refinement.

5.2. *Uniform flow around a circular cylinder*

5.2.1. Problem statement. The computational domain and boundary conditions for this problem are shown in Figure 3(a). Because the problem is 2D only a slab was meshed with 3D tetrahedral elements. The mesh is shown in Figure 3(b) and was designed to provide adequate refinement in the boundary layer where gradients are higher and in the wake of the cylinder where the solution is expected to exhibit larger time variations. A steady velocity profile was imposed at the inflow. The first computations were carried out for a Reynolds number $Re = \rho U_0 d/\mu$ equal to 100, for which a vortex street forms in the wake of the cylinder. Because the computational domain and mesh are symmetrical, the vortex street is determined by truncation errors and non-linear iterative convergence parameters which are difficult to characterize and use as model parameters. To provide a rigorous controlled framework to investigate the vortex street sensitivities, we use a perturbation of the uniform velocity profile as a trigger mechanism for vortex formation. The inflow velocity is given by

$$U_f = U_0(1 + U_p g(y)) \tag{30}$$

where $U_0 = 1$ is the value of the free-stream velocity, U_p is a small velocity perturbation set to 10^{-3} and $g(y)$ is an anti-symmetric function taking values between -1 and 1. Here we have used the form:

$$g(y) = \tanh(\beta y) \tag{31}$$

with $\beta = 10$. This approach ensures that small changes in parameter values will induce small changes in the behaviour of the flow.

The initial conditions are obtained from a steady-state solution of the flow and sensitivity equations. Following the work of Sohankar, the time step is set to $\Delta t = 0.025$ [33]. This leads to

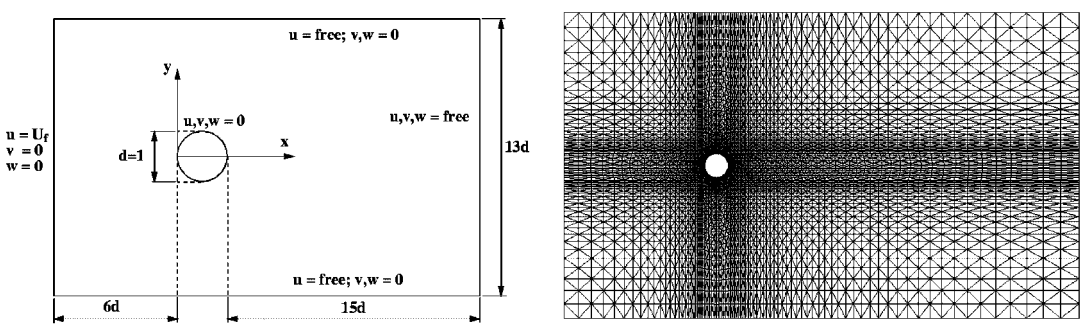

Figure 3. Uniform flow around a circular cylinder; definition and mesh: (a) domain and boundary conditions and (b) mesh.

DOI: 10.1002/fld

about 240 time steps per period of vortex shedding. Sensitivities are computed with respect to the inlet velocity U_0. The only non-zero boundary condition for the sensitivities are those at the inlet.

5.2.2. Flow response. The initial solution of the transient problem is symmetrical (see the vorticity contours in Figure 4). Figure 5 shows the time variation of the flow (velocity and pressure) at a point located on the symmetry axis one diameter downstream of the cylinder. The signal is shown for time $t = 0$–160. Notice that during the first part of the simulation the transverse velocity v

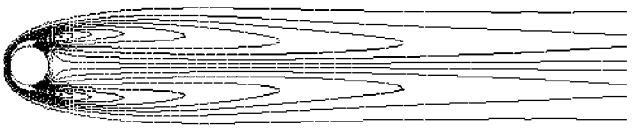

Figure 4. Uniform flow around a circular cylinder: vorticity contours of initial solution.

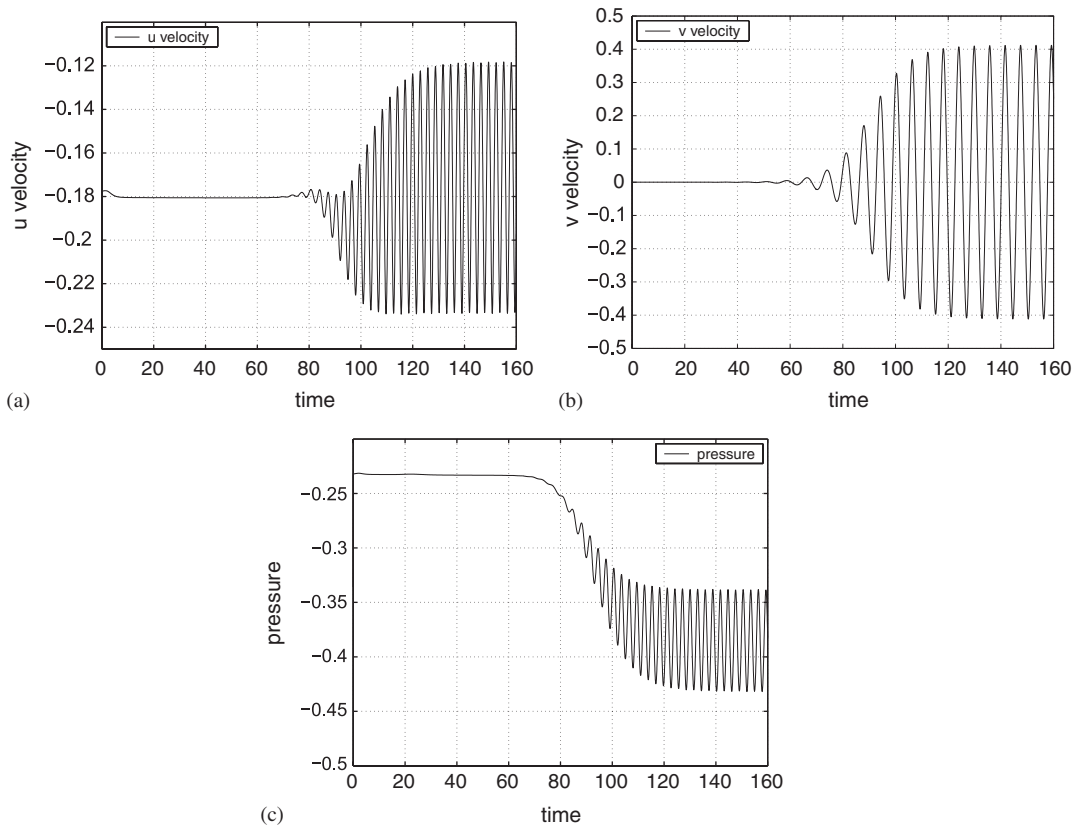

Figure 5. Uniform flow around a circular cylinder; flow response at $(x = 2, y = 0)$: (a) u-velocity; (b) v-velocity; and (c) pressure.

DOI: 10.1002/fld

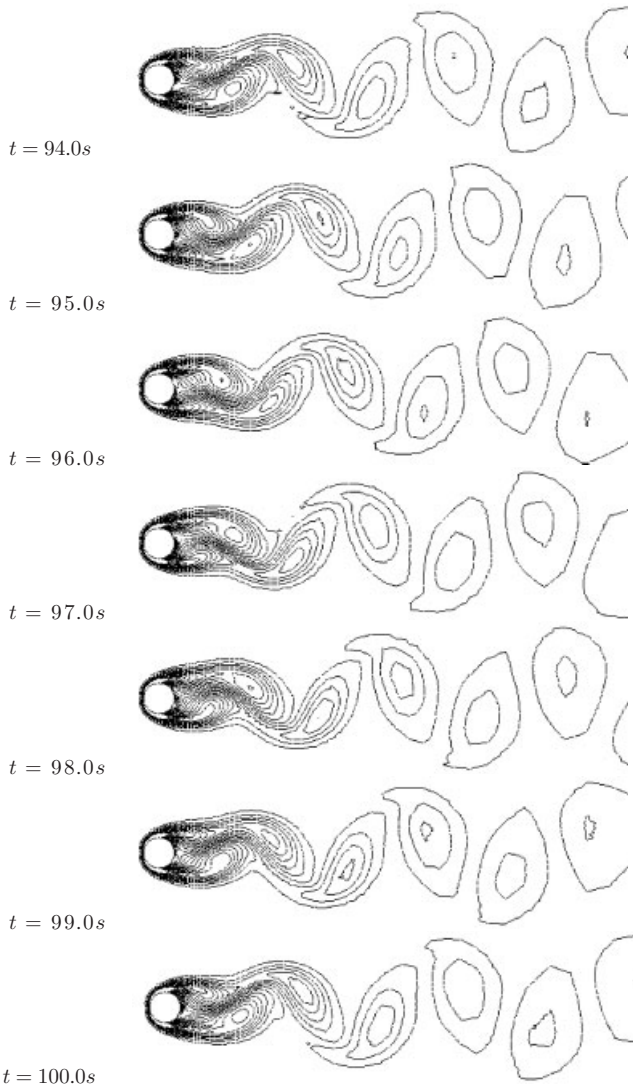

Figure 6. Uniform flow around a circular cylinder: Karman vortex street.

is zero, confirming that the flow is symmetric with respect to the x-axis. The axial velocity u and the pressure p are also constant until approximately $t = 60$, after which time perturbations are observed and the solution is no longer symmetrical. The amplitude of these perturbations increases in time and leads to the formation of the well-known Karman vortex street. This is to be expected as the wake of a circular cylinder at $Re = 100$ is an unstable flow. Because the critical Reynolds number for this flow is $Re_{\text{cr}} = 51$ [33], in principle a vortex street should develop for constant inflow boundary conditions. Vorticity contours are shown in Figure 6 for $t = 94$–100 clearly illustrating the Karman vortex street in the wake of the cylinder.

DOI: 10.1002/fld

5.2.3. Flow sensitivity responses. The first- and second-order sensitivities represent the slope and curvature of the dependent variables in parameter space. Their time signals at $(x=2, y=0)$ for U_0 as parameter are shown in Figure 7. The following observations can be made:

- The period of the sensitivity signals is the same as the period of the flow.
- Sensitivity perturbations from the steady-state solution occur around $t=60$ as was the case for the flow variables.
- Time signal of the flow variables exhibits constant amplitude periodic behaviour, whereas the sensitivities show an unbounded increase in the signal amplitude.
- The amplitude of the sensitivities is much higher than the amplitude of the flow variables. For example at $t=100$ the v-velocity amplitude has almost reached its maximum value, whereas the amplitude of the first-order sensitivity is about 10^2 times larger and that of the second-order sensitivity is 10^4 times larger and they keep increasing with time.

Additional verification of the computed sensitivities can be done by estimating the flow gradients with respect to U_0 by finite differences (FDs). For this, the inlet velocity U_0 is changed by a small amount δU_0 and the solution is recomputed. The reference finite difference flow sensitivities are determined from

$$\left(\frac{\partial \mathbf{u}}{\partial U_0}\right)_{\mathrm{FD}} = \frac{\mathbf{u}(U_0+\delta U_0)-\mathbf{u}(U_0-\delta U_0)}{2\delta U_0} + \mathcal{O}(\delta U_0^2) \tag{32}$$

$$\left(\frac{\partial^2 \mathbf{u}}{\partial U_0^2}\right)_{\mathrm{FD}} = \frac{\mathbf{u}(U_0+\delta U_0)-2\mathbf{u}(U_0)+\mathbf{u}(U_0-\delta U_0)}{\delta U_0^2} + \mathcal{O}(\delta U_0^2) \tag{33}$$

in which δU_0 is taken very small compared to U_0. The authors have shown in previous work [34] that the first- and second-order sensitivities compare very well with gradients computed by FDs for a pulsed flow around a square cylinder. Note however that the error of the gradient estimated using FDs depends on the magnitude of higher-order derivatives. The $\mathcal{O}(\delta U_0^2)$ terms in (32) and (33) contain the third-order derivative of the solution in the case of the first-order sensitivity and the fourth-order derivative of the solution for the second-order sensitivity. For the present problem, the high-order derivatives have magnitudes which increase very rapidly with time as shown in the next sub-section. The magnitude of the third-order derivative increase with the third power of time and the fourth-order derivative with the fourth power of time. This makes FD derivatives inaccurate at latter times especially for the second-order derivative. One way to increase the accuracy of FD gradients may be to decrease the perturbation δU_0. The improvement is however very limited as a decrease of δU_0 magnifies the errors introduced by the finite accuracy of the finite element solution (the solutions were converged down to a relative error of 10^{-8}). To illustrate this point, Figure 8 compares the continuous sensitivities of the vertical velocity v with FD estimations using $\delta U_0 = 0.01U_0$ and $\delta U_0 = 0.001U_0$, respectively. As can be seen, the FD estimates are different for different values of the perturbation δU_0. This indicates that the FD estimate is not reliable enough and cannot be used as a standard to evaluate the accuracy of the continuous sensitivities. For the first-order sensitivity, the CSE solution compares very well with the FD gradient obtained for $\delta U_0 = 0.001U_0$. For the second-order sensitivity, the agreement is better when comparing with the FD gradient using $\delta U_0 = 0.01U_0$.

DOI: 10.1002/fld

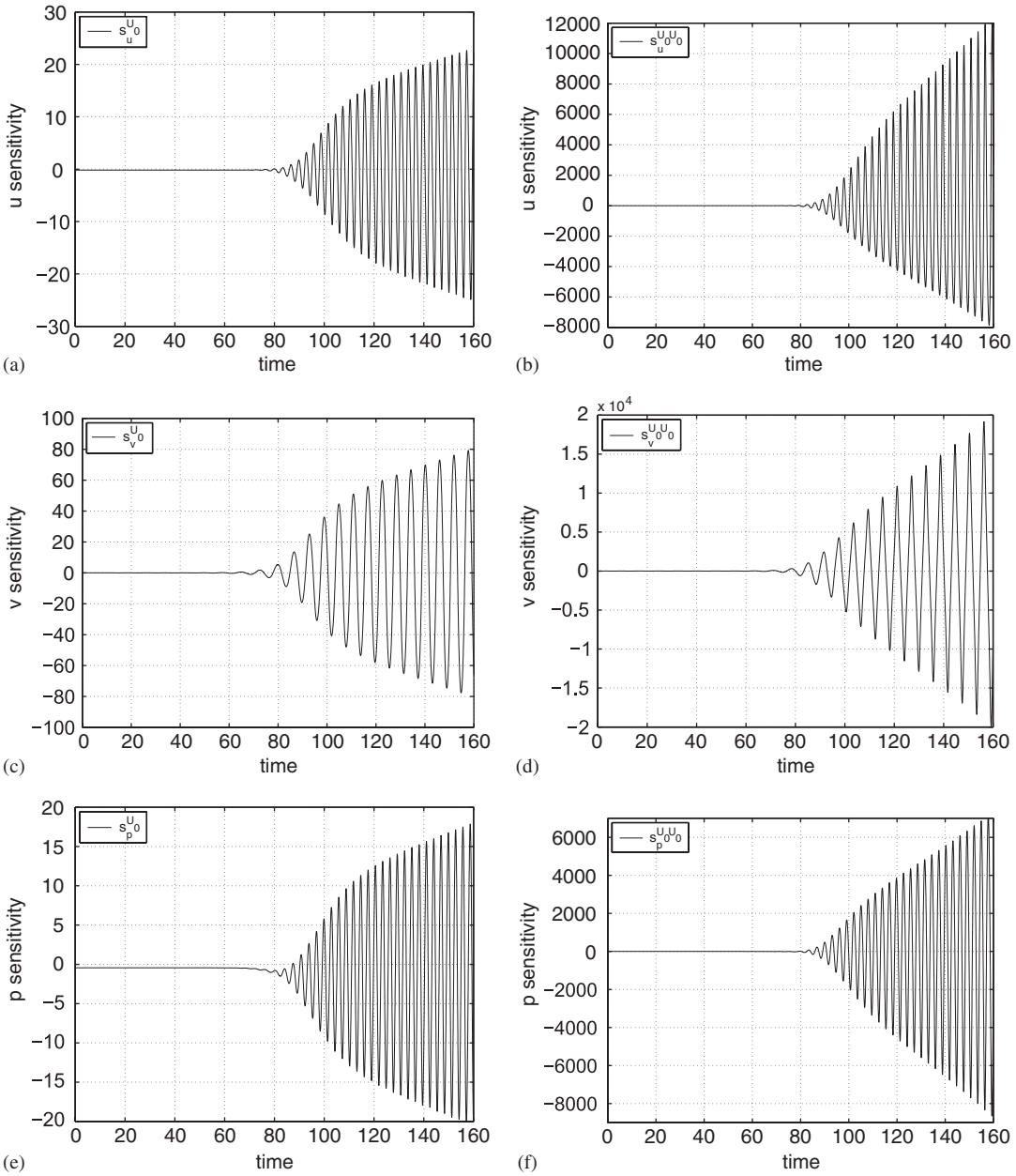

Figure 7. Uniform flow around a circular cylinder; sensitivities with respect to U_0 at $(x = 2.0, y = 0.0)$: (a) $s_u^{U_0}$; (b) $s_u^{U_0U_0}$; (c) $s_v^{U_0}$; (d) $s_v^{U_0U_0}$; (e) $s_p^{U_0}$; and (f) $s_p^{U_0U_0}$.

DOI: 10.1002/fld

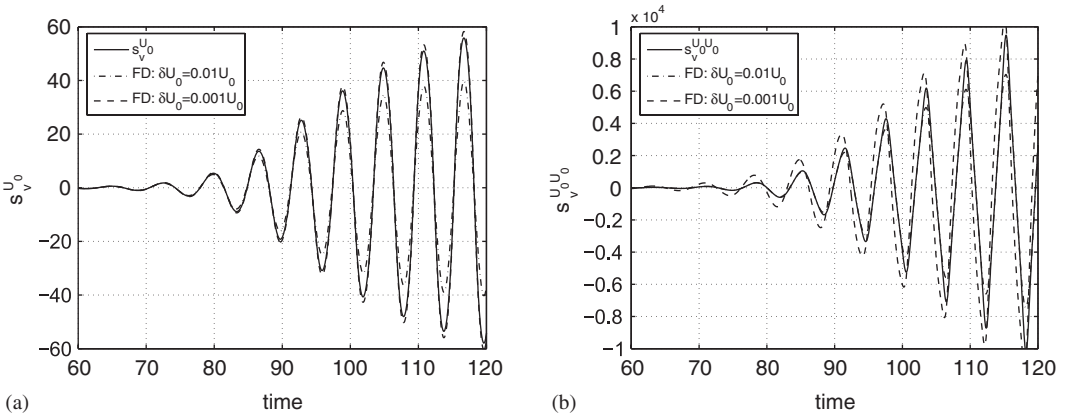

Figure 8. Comparison of CSE and FD sensitivities of v at ($x = 2.0$, $y = 0.0$): (a) $s_v^{U_0}$ and (b) $s_v^{U_0U_0}$.

5.2.4. Fast evaluation of nearby flows. Sensitivities can be used for fast evaluation of nearby flows. The prediction of nearby flows of periodic solutions having an infinite number of derivatives defined is very challenging. Consider for example what happens to the v-velocity, when a generic parameter a is subjected to a variation δa from its nominal value a_0. The Taylor series expansion reads

$$v(x, y; a_0 + \delta a) = v(x, y; a_0) + \frac{\partial v}{\partial a}\,\delta a + \frac{\partial^2 v}{\partial a^2}\,\frac{\delta a^2}{2} + O(\delta a^3) \tag{34}$$

We compare the quadratic Taylor approximation of u, v and p to a full flow analysis at the perturbed values of the parameter.

The observation made in the previous section that the amplitude of the sensitivities increases continuously with time is of particular importance since it indicates that, as time advances, the second-order terms will increase in importance to eventually become dominant in Equation (34). To better understand this behaviour of the sensitivity solution, consider the v-velocity in the fully established periodic region ($t > 120$) as given by a sinusoidal function with amplitude v_m and frequency f both depending on the inlet velocity:

$$v(t; U_0) = v_m(U_0)\sin(2\pi f(U_0)t) \tag{35}$$

The sensitivities of v with respect to U_0 are obtained by differentiating (35) as follows:

$$s_v^{U_0} = \frac{\partial v}{\partial U_0} = \frac{\partial v_m}{\partial U_0}\,\sin(2\pi f t) + v_m\left(2\pi\frac{\partial f}{\partial U_0}t\right)\cos(2\pi f t) \tag{36}$$

$$\begin{aligned} s_v^{U_0U_0} = \frac{\partial^2 v}{\partial U_0^2} = \frac{\partial^2 v_m}{\partial U_0^2}\,\sin(2\pi f t) + 2\frac{\partial v_m}{\partial U_0}\left(2\pi\frac{\partial f}{\partial U_0}t\right)\cos(2\pi f t) \\ -v_m\left(2\pi\frac{\partial f}{\partial U_0}t\right)^2\sin(2\pi f t) + v_m\left(2\pi\frac{\partial^2 f}{\partial U_0^2}t\right)\cos(2\pi f t) \end{aligned} \tag{37}$$

DOI: 10.1002/fld

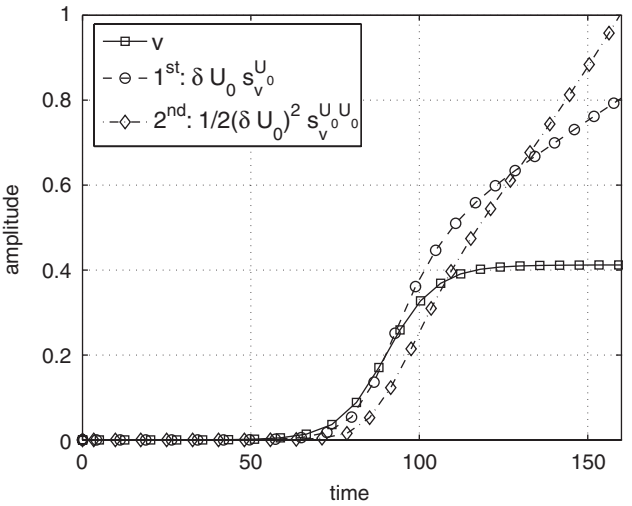

Figure 9. Amplitude of the terms in the Taylor series expansion for v.

Note that the amplitude of the second term on the right-hand side of Equation (36) increases linearly with time. The second-order sensitivity has contributions that increase linearly and quadratically with time. It is clear that as time increases those terms will become dominant and determine how the sensitivities amplitude will vary with time. Equations (36) and (37) also indicate that the amplitude of the sensitivity signals is proportional to that of the flow variable. This explains why the sensitivities of the v-velocity have higher amplitudes than those of the u-velocity and of the pressure (see Figure 7).

For illustration purposes, we consider a perturbation of 1% of the inflow velocity. The magnitude of the various terms in the Taylor expansion is illustrated in Figure 9 for the v-velocity at $(x=2, y=0)$. The figure shows the time evolution of the amplitude of the velocity v and of the first- and second-order terms, $(\partial v/\partial a)\delta a$ and $(\partial^2 v/\partial a^2)(\delta a^2/2)$. For this value of the increment δU_0, the amplitude of the first-order term is comparable to the amplitude of v up to $t=90$. At later times, the amplitude of the first-order term is higher than the amplitude of the solution itself. The second-order term becomes sizable compared to the first-order term at a time around $t=70$. This indicates that second-order derivatives are very important to obtain accurate estimates of nearby solutions for $t>70$. The magnitude of the first- and second-order terms become comparable to that of v itself around $t=100$. It is expected that higher-order terms (3 and higher) will also become important at later times ($t>100$). In conclusion, the Taylor series extrapolation for $\delta U_0 = 0.01 U_0$ can only be performed until $t=100$. The time interval over which the Taylor series extrapolation produces reliable predictions increases with decreasing values of the perturbation.

Results obtained using first- and second-order Taylor series are shown in Figure 10 for the point $(x=2, y=0)$ and a time interval between $t=60$ and 100. At early times, the two Taylor series approximations of the flow response are in good agreement with the CFD re-analysis at the perturbed value of the parameter $(U_0 + \delta U_0)$. As expected given the size of higher-order terms, the agreement deteriorates with time especially at $t>80$. The agreement is better for the

DOI: 10.1002/fld

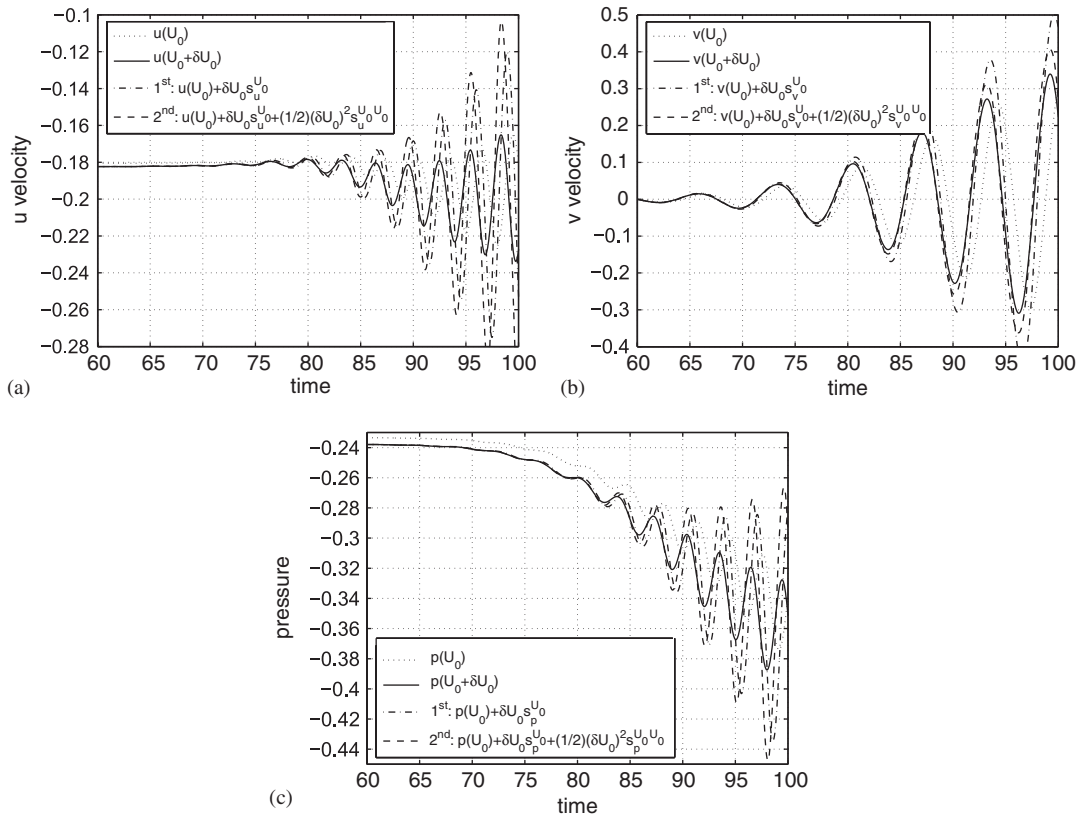

Figure 10. Uniform flow around a circular cylinder; fast nearby solutions for δU_0 equal to 1% of U_0 at ($x = 2.0$, $y = 0.0$): (a) $u(U_0 + \delta U_0)$, $\delta U_0 = 0.01 U_0$; (b) $v(U_0 + \delta U_0)$, $\delta U_0 = 0.01 U_0$; and (c) $p(U_0 + \delta U_0)$, $\delta U_0 = 0.01 U_0$.

vertical velocity v which exhibits larger amplitude than u and p. In all cases the second-order Taylor series provides better agreement with the re-analysis than the first-order one. Observe also that the second-order reconstruction is in better phase with the true solution than the first-order reconstruction.

Figure 11 presents the spatial distributions of the v-velocity extrapolations obtained by the Taylor series for $\delta U_0 = 0.01 U_0$ compared to those obtained by a full flow reanalysis. Comparisons are shown for a station located at $x = 4$, and time ranging from $t = 75$–80. The baseline solution at the unperturbed value of the parameter is also shown, so that the effect of increasing the order of the Taylor series can be assessed. Results indicate that the accuracy of the extrapolation is much improved when second-order terms are used. In all cases second-order Taylor series extrapolations are almost superimposed over the recomputed solution, whereas first-order Taylor extrapolations exhibit higher errors. Observe also that some particular characteristics of the solution, such as the knee in the velocity profile at $y = 1$ and $t = 78$ (Figure 11(d)) are well captured by the second-order Taylor series, but are entirely missed by first-order approximation.

DOI: 10.1002/fld

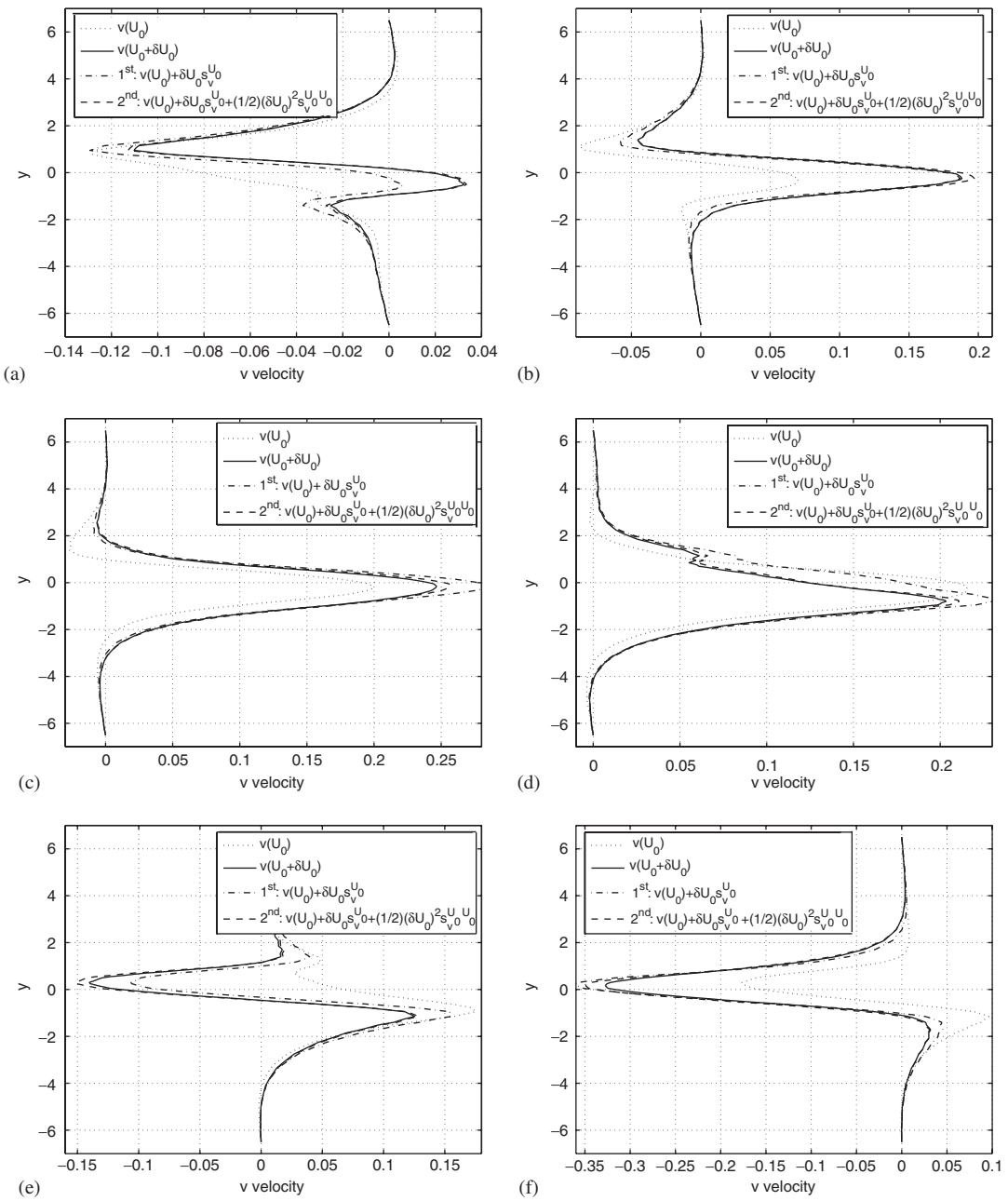

Figure 11. Circular cylinder in uniform flow at $x = 4.0$; extrapolated and true profiles of v for $\delta U_0 = 0.01 U_0$: (a) v component at $t = 75$; (b) v component at $t = 76$; (c) v component at $t = 77$; (d) v component at $t = 78$; (e) v component at $t = 79$; and (f) v component at $t = 80$.

DOI: 10.1002/fld

5.2.5. Sensitivity of the Strouhal number. The frequency of the vortex shedding was analysed by computing the Strouhal number:

$$St = \frac{fD}{U_0} \tag{38}$$

where f is the frequency of the vortex shedding and D is the diameter of the cylinder. The Strouhal number is known to depend upon the Reynolds number of the flow and a correlation of experimental data for the Strouhal–Reynolds relationship was proposed by Williamson [35]. Here, the solution given by the present numerical approach is compared to the correlation by Williamson. The sensitivity of the Strouhal number with respect to the Reynolds number was computed as follows:

$$\frac{\partial St}{\partial Re} = \lim_{\delta Re \to 0} \frac{St[\mathbf{u}(Re + \delta Re)] - St[\mathbf{u}(Re - \delta Re)]}{2\delta Re} \tag{39}$$

$$\frac{\partial^2 St}{\partial Re^2} = \lim_{\delta Re \to 0} \frac{St[\mathbf{u}(Re + \delta Re)] - 2St[\mathbf{u}(Re)] + St[\mathbf{u}(Re - \delta Re)]}{(\delta Re)^2} \tag{40}$$

with the Strouhal number obtained from the following two Taylor expansions:

$$St[\mathbf{u}(Re + \delta Re)] = St[\mathbf{u}(Re) + \mathbf{s}_u^{Re}\delta Re + \tfrac{1}{2}\mathbf{s}_u^{ReRe}(\delta Re)^2] \tag{41}$$

$$St[\mathbf{u}(Re - \delta Re)] = St[\mathbf{u}(Re) - \mathbf{s}_u^{Re}\delta Re + \tfrac{1}{2}\mathbf{s}_u^{ReRe}(\delta Re)^2] \tag{42}$$

Sensitivities of the flow with respect to the Reynolds number are obtained from the sensitivity of the flow with respect to the free-stream velocity U_0 as

$$\mathbf{s}_u^{Re} = \frac{U_0}{Re}\,\mathbf{s}_u^{U_0} \tag{43}$$

$$\mathbf{s}_u^{ReRe} = \left(\frac{U_0}{Re}\right)^2 \mathbf{s}_u^{U_0U_0} \tag{44}$$

The computed values of the Strouhal number and of its first- and second-order derivatives with respect to the Reynolds number are given in Table III for $Re = 80$, 100 and 125.

Results are shown in Figure 12. Two sets of numerical solutions are plotted. The first one, identified as Mesh 1, corresponds to the solution obtained on a domain of the size shown in Figure 3(a). Behr *et al.* [36] reported that St depends on the location of the upper and lower boundaries. Therefore, a second series of computations was carried out on a domain twice as high

Table III. Results for the uniform flow around a circular cylinder (Mesh 2).

Re	80	100	125
St	0.1573	0.1685	0.1786
$\partial St/\partial Re$	0.633×10^{-3}	0.446×10^{-3}	0.314×10^{-3}
$\partial^2 St/\partial Re^2$	-1.11×10^{-5}	-0.73×10^{-5}	-0.38×10^{-5}

DOI: 10.1002/fld

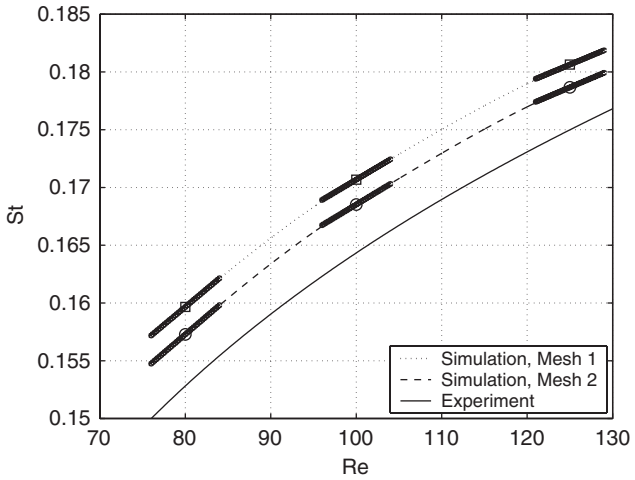

Figure 12. Uniform flow around a circular cylinder: Strouhal dependence upon Reynolds.

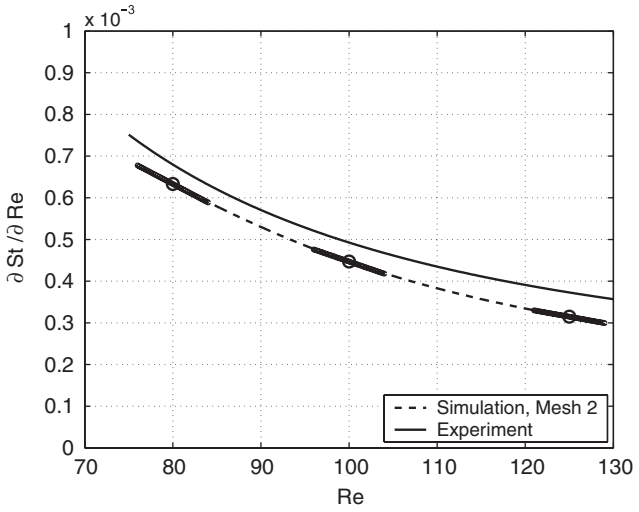

Figure 13. Uniform flow around a circular cylinder: variation of the slope $\partial St/\partial Re$ with Re.

as that of Figure 3(a) (Mesh 2). The solution exhibits little dependence to further changes in the location of the boundary [36]. As can be seen, the numerical solution overestimates the experimental correlation, but the difference decreases when larger domains are used, mostly due to a better approximation of the infinite domain. Note also that the gap between the simulated St and the experimental correlation remains constant with changes in the Reynolds number. This indicates that the simulation reproduces the changes in St due to changes in Re. The sensitivity of the Strouhal number with respect to Re was also computed by using Equations (39) and (40). The sensitivity is in fact the slope of the St–Re curve and is shown in Figure 12 with thicker lines

DOI: 10.1002/fld

around the solution computed at *Re* numbers of 80, 100 and 125. As can be seen, the SEM produces results that correctly describe the trend in the *St–Re* relationship. The slope of *St* computed from the sensitivities agrees very well with that of the computed and experimental *St–Re* relationships.

Comparison between the values of $\partial St/\partial Re$ given by the experimental correlation and the sensitivity analysis are shown in Figure 13 for Mesh 2. The second-order derivative $\partial^2 St/\partial Re^2$ computed from the solution sensitivities is the slope of the $\partial St/\partial Re$ *vs Re* curve (thicker lines in Figure 13). Here again we see that the agreement is good with the experimental observation. Note that the second-order derivative $\partial^2 St/\partial Re^2$ can only be obtained by solving for the second-order sensitivities of the flow.

6. CONCLUSION

A general sensitivity equation formulation was developed for computing first- and second-order sensitivities of time-dependent incompressible laminar flows. The method was verified on a problem with a closed-form solution to confirm the rate of convergence of the flow and sensitivity solvers.

The method was then applied to the flow around a circular cylinder. The flow starts with a symmetrical solution and then goes through a transition phase leading to the usual Karman vortex street characterized by alternate vortex shedding. The Taylor series expansions in parameter space using sensitivities were shown to be a powerful tool for fast evaluation of nearby flows. Results indicate that accuracy improves when second-order sensitivities are included in the Taylor series expansions.

Flow sensitivities were used to determine the sensitivity of the Strouhal number with respect to the Reynolds number. The slope of the *St–Re* relationship $\partial St/\partial Re$ and curvature $\partial^2 St/\partial Re^2$ computed using sensitivity information agree well with both the computed and experimental observations of the dependence of *St* on *Re*.

ACKNOWLEDGEMENTS

This work was sponsored in part by NSERC (Government of Canada), the Canada Research Chair Program (Government of Canada) and by the Air Force Office of Scientific Research under grant AFOSR F49620-00-1-0299.

REFERENCES

1. Roache PJ. *Verification and Validation in Computational Science and Engineering*. Hermosa: Albuquerque, NM, 1998.
2. Martins JRRA, Stradza P, Alonso JJ. The complex-step derivative approximation. *ACM Transactions on Mathematical Software—TOMS* 2003; **29**(3):245–262.
3. Putko M, Newman P, Taylor A, Green L. Approach for uncertainty propagation and robust design in CFD using sensitivity derivatives. *Fifteenth AIAA Computational Fluid Dynamics Conference*, *AIAA Paper 2001-2528*, Anaheim, CA, June 2001.
4. Borggaard J, Burns J. A PDE sensitivity equation method for optimal aerodynamic design. *Journal of Computational Physics* 1997; **136**(2):366–384.
5. Stanley LG, Stewart DL. *Design Sensitivity Analysis*: *Computational Issues of Sensitivity Equation Methods*. Frontiers in Applied Mathematics, vol. 25. SIAM: Philadelphia, 2001.
6. Turgeon É, Pelletier D, Borggaard J. A general continuous sensitivity equation formulation for complex flows. *Numerical Heat Transfer*, *Part B* 2002; **42**:485–498.

DOI: 10.1002/fld

7. Haug EJ, Choi K, Komkov V. *Design Sensitivity Analysis of Structural Systems*. Mathematics in Science and Engineering, vol. 17. Academic Press: Orlando, 1986.
8. Hien TD, Kleiber M. Stochastic finite element modeling in linear heat transfer. *Computer methods in Applied Mechanics and Engineering* 1997; **144**:111–124.
9. Gunzburger MD. *Perspectives in Flow Control and Optimization*. SIAM: Philadelphia, 2002.
10. Sherman LL, Taylor III AC, Green L, Newman PA, Hou GW, Korivi VM. First- and second-order aerodynamic sensitivity derivatives via automatic differentiation. *Journal of Computational Physics* 1996; **129**(2):307–331.
11. Godfrey AG, Cliff EM. Direct calculation of aerodynamic force derivatives: a sensitivity-equation approach. *Thirty-sixth AIAA Aerospace Sciences Meeting and Exhibit*, *AIAA Paper 98-0393*, Reno, NV, January 1998.
12. Godfrey AG, Cliff EM. Sensitivity equations for turbulent flows. *Thirty-ninth AIAA Aerospace Sciences Meeting and Exhibit*, *AIAA Paper 2001-1060*, Reno, NV, January 2001.
13. Limache A. Aerodynamic modeling using computational fluid dynamics and sensitivity equations. *Ph.D. Thesis*, Virginia Polytechnic Institute and State University, Blacksburg, VA, 2000.
14. Turgeon É, Pelletier D, Borggaard J. Computation of airfoil flow derivatives using a continuous sensitivity equation method. *Eighth CASI Aerodynamics Symposium*, Toronto, Canada, April 2001.
15. Blackwell BF, Dowding KJ, Cochran RJ, Dobranich D. Utilization of sensitivity coefficients to guide the design of a thermal battery. *Proceedings of the 1998 ASME/IMECE*, ASME, HTD-vol. 561–5, Anaheim, CA, 1998; 73–82.
16. Borggaard J, Pelletier D. Optimal shape design in forced convection using adaptive finite elements. *Thirty-Sixth AIAA Aerospace Sciences Meeting and Exhibit*, *AIAA Paper 98-0908*, Reno, NV, January 1998.
17. Turgeon É, Pelletier D, Borggaard J. A general purpose sensitivity equation formulation for complex flows. *Proceedings of the 8th Annual Conference of the Computational Fluid Dynamics Society of Canada*, vol. 2, Montréal, Canada, 11–13 June 2000; 697–704.
18. Turgeon É, Pelletier D, Borggaard J. Applications of continuous sensitivity equations to flows with temperature-dependent properties. *Numerical Heat Transfer*, *Part A*: *Applications* 2003; **44**:611–624.
19. Turgeon É, Pelletier D, Borggaard J. Application of a sensitivity equation method to the k–ε model of turbulence. *Fifteenth AIAA Computational Fluid Dynamics Conference*, *AIAA Paper 2001-2534*, Anaheim, CA, June 2001.
20. Turgeon É, Pelletier D, Borggaard J. A general continuous sensitivity equation formulation for the k–ε model of turbulence. *Thirty-first AIAA Fluid Dynamics Conference and Exhibit*, *AIAA Paper 2001-3000*, Anaheim, CA, June 2001.
21. Ilinca F, Hétu J-F. Three-dimensional simulation and design sensitivity analysis of the injection molding process. *NUMIFORM 2004*, Columbus, OH, June 2004.
22. Turgeon É, Pelletier D, Borggaard J. A continuous sensitivity equation approach to optimal design in mixed convection. *Thirty-third AIAA Thermophysics Conference*, *AIAA Paper 99-3625*, Norfolk, VA, June–July 1999.
23. Turgeon É, Pelletier D, Borggaard J. Sensitivity and uncertainty analysis for variable property flows. *Thirty-ninth AIAA Aerospace Sciences Meeting and Exhibit*, *AIAA Paper 2001-0139*, Reno, NV, January 2001.
24. Hristova H, Étienne S, Pelletier D, Borggaard J. A continuous sensitivity equation method for time-dependent incompressible laminar flows. *International Journal for Numerical Methods in Fluids* 2006; **50**:817–844.
25. Mahieu J-N, Étinne S, Pelletier D, Borggaard J. A second-order sensitivity equation method for laminar flow. *International Journal of Computational Fluid Dynamics* 2005; **19**:143–157.
26. Hughes TJR, Franca LP, Balestra M. A new finite element formulation for computational fluid dynamics: V. Circumventing the Babuška–Brezzi condition: a stable Petrov–Galerkin formulation of the Stokes problem accommodating equal-order interpolations. *Computer Methods in Applied Mechanics and Engineering* 1986; **59**:85–99.
27. Hughes TJR, Franca LP, Hulbert GM. A new finite element formulation for computational fluid dynamics: VII. The Galerkin-least-squares method for advective–diffusive equations. *Computer Methods in Applied Mechanics and Engineering* 1989; **73**:173–189.
28. Franca LP, Frey SL. Stabilized finite element methods: II. The incompressible Navier–Stokes equations. *Computer Methods in Applied Mechanics and Engineering* 1992; **99**(2–3):209–233.
29. Ilinca F, Hétu J-F, Pelletier D. On stabilized finite element formulations for incompressible flows. *Thirteenth AIAA Computational Fluid Dynamics Conference*, *AIAA Paper 97-1863*, Snowmass, Colorado, 1997.
30. Tezduyar TE, Shih R, Mittal S, Ray SE. Incompressible flow using stabilized bilinear and linear equal-order-interpolation velocity–pressure elements. *Research Report UMSI 90/165*, University of Minnesota/Supercomputer Institute, Minneapolis, 1990.

DOI: 10.1002/fld

31. Tezduyar TE, Aliabadi SK, Behr M, Mittal S. Massively parallel finite element simulation of compressible and incompressible flows. *Research Report 94-013*, Army High Performance Computing Research Center, Minneapolis, MN, 1994.
32. Von Schwind JJ. *Geophysical Fluid Dynamics for Oceanographers*. Prentice-Hall: Englewood Cliffs, NJ, 1980.
33. Sohankar A, Norberg C, Davidson L. Low-Reynolds-number flow around a square cylinder at incidence: study of blockage, onset of vortex shedding and outlet boundary condition. *International Journal for Numerical Methods in Fluids* 1998; **26**:39–56.
34. Ilinca F, Pelletier D, Borggaard J. A continuous second-order sensitivity equation method for time-dependent incompressible laminar flows. *Seventeenth AIAA Computational Fluid Dynamics Conference*, *AIAA Paper 2005-5252*, Toronto, ON, 2005.
35. Williamson CHK. Defining a universal and continuous Strouhal–Reynolds number relationship for the laminar vortex shedding of a circular cylinder. *Physics of Fluids* 1988; **31**:2742–2744.
36. Behr M, Hastreiter D, Mittal S, Tezduyar TE. Incompressible flow past a circular cylinder: dependence of the computed field on the location of the lateral boundaries. *Computer Methods in Applied Mechanics and Engineering* 1995; **123**:309–316.

DOI: 10.1002/fld